Core–Shell Li3V2(PO4)3@C Composites as Cathode Materials for Lithium-Ion Batteries

ARTICLE *in* THE JOURNAL OF PHYSICAL CHEMISTRY C · MARCH 2008

Impact Factor: 4.77 · DOI: 10.1021/jp800040s

5 AUTHORS, INCLUDING:

Mengyu Ren
Sun Yat-Sen University
48 PUBLICATIONS **641** CITATIONS
SEE PROFILE

Zhen Zhou
Nankai University
211 PUBLICATIONS **6,657** CITATIONS
SEE PROFILE

Core−Shell $Li_3V_2(PO_4)_3$@C Composites as Cathode Materials for Lithium-Ion Batteries

M. M. Ren, Z. Zhou,* X. P. Gao, W. X. Peng, and J. P. Wei

Institute of New Energy Material Chemistry, Nankai University, Tianjin 300071, China

Received: January 3, 2008; In Final Form: January 23, 2008

Core−shell $Li_3V_2(PO_4)_3$@C nanostructured composites were prepared via a sol−gel route followed by hydrothermal treatment. XRD patterns showed that $Li_3V_2(PO_4)_3$ has a monoclinic structure with space group $P2_1/n$. TEM images exhibited that $Li_3V_2(PO_4)_3$ particles are encapsulated with a carbon shell ∼10 nm in thickness. Compared with pure $Li_3V_2(PO_4)_3$, core−shell $Li_3V_2(PO_4)_3$@C composites presented enhanced electrochemical Li ion intercalation performances. Cyclic voltammetry and electrochemical impedance spectroscopy disclosed that carbon shells improved Li ion diffusion and electrical conductance significantly and also retarded formation of solid electrolyte interphase film of $Li_3V_2(PO_4)_3$ cathode materials.

1. Introduction

Lithium-ion batteries are the most important power sources for the increasing demand from portable electronic products, electrical vehicles, hybrid electrical vehicles, etc. The current commercial cathode material, $LiCoO_2$, possesses some problems in large-scale utilization, such as high cost and safety issues. Another class of Li intercalation materials, transition-metal phosphates, exemplified by $LiMPO_4$ (M = Fe, Co, Ni, Mn),[1−9] $Li_3V_2(PO_4)_3$,[10−18] and $LiVPO_4F$,[19−21] has been proposed as next-generation cathode materials for Li-ion batteries because they contain both mobile Li ions and redox-active metals within a rigid phosphate network, displaying remarkable electrochemical and thermal stability.

Among the above-mentioned phosphates, monoclinic lithium vanadium phosphate, α-$Li_3V_2(PO_4)_3$, is a promising cathode material for Li-ion batteries. It contains three independent lithium sites with a theoretical discharge capacity of 197 mAh g^{-1}, while three Li ions are completely extracted up to 4.8 V.[10] However, $Li_3V_2(PO_4)_3$ has low electrical conductivity as $LiFePO_4$. This problem can be solved to some degree by metal doping or mixing with electrically conductive materials such as carbon.[12,13] In particular, carbon coating is regarded as an effective way toward improving the performance of $Li_3V_2(PO_4)_3$, but it is rather difficult to encapsulate $Li_3V_2(PO_4)_3$ homogeneously with a carbon shell during the formation procedure of $Li_3V_2(PO_4)_3$ at high temperatures. Also, excessive carbon decreases the filling density of active substances in the cathodes.

More recently, materials with core−shell structures have been introduced to the field of Li-ion batteries.[22,23−33] Core−shell materials used in Li-ion batteries are expected to combine the functions of both core and shell parts and then improve the general performance of the composites. In this work, $Li_3V_2(PO_4)_3$ was synthesized initially via a sol−gel route, and subsequently, a posthydrothermal treatment was adopted to form a carbon shell in the surface of $Li_3V_2(PO_4)_3$ particles. The electrochemical Li-ion intercalation performance was compared between $Li_3V_2(PO_4)_3$@C composites and pure $Li_3V_2(PO_4)_3$.

* To whom correspondence should be addressed. E-mail: zhouzhen@nankai.edu.cn (Z.Z.).

2. Experimental Section

2.1. Preparation of Pure $Li_3V_2(PO_4)_3$ and $Li_3V_2(PO_4)_3$@C Composites. Pure $Li_3V_2(PO_4)_3$ was synthesized using V_2O_5, $NH_4H_2PO_4$, Li_2CO_3, and oxalic acid as starting materials. Oxalic acid was used here not only as a chelating regent but also as a reducing agent. First, oxalic acid and V_2O_5 in a stoichiometric ratio were dissolved in deionized water with magnetic stirring at 70 °C. After a clear blue solution formed (eq 1), a mixture of stoichiometric $NH_4H_2PO_4$ and Li_2CO_3 was added to the solution while stirring for 4 h, and then a gel formed in an air oven at 100 °C. The gel was decomposed at 350 °C in an argon atmosphere for 4 h, and the obtained product was ground, pressed into pellets, and sintered at 750 °C for 4 h in flowing argon (eq 2). The sample was divided into two parts: one was further heated at 750 °C for 2 h in an argon atmosphere; the other was used to prepare $Li_3V_2(PO_4)_3$@C composites via a posthydrothermal procedure, as described in detail as follows. The as-prepared $Li_3V_2(PO_4)_3$ (1.0 g) was transferred to a clear solution of 0.5 g of glucose dissolved in 40 mL of deionized water. The mixture was placed in a 50 mL Teflon-sealed autoclave and maintained at 180 °C in a muffle for 3 h, since glucose is carbonized at 180 °C under hydrothermal conditions.[34] The product was centrifuged and washed with deionized water for at least five times and dried in oven at 100 °C for 8 h, and finally the powder was also sintered at 750 °C for 2 h in flowing argon.

$$V_2O_5 + 3H_2C_2O_4 \rightarrow 2VOC_2O_4 + 3H_2O + 2CO_2 \quad (1)$$

$$4VOC_2O_4 + 3Li_2CO_3 + 6NH_4H_2PO_4 \rightarrow 2Li_3V_2(PO_4)_3 + 9CO_2 + 2CO + 6NH_3 + 9H_2O \quad (2)$$

2.2. Sample Characterization. X-ray diffraction (XRD) patterns of the samples were measured using a Rigaku D/Max III diffractometer with Cu Kα radiation (λ = 1.5418 Å). The samples were observed using a Hitachi S-3500N scanning electron microscope (SEM) and a FEI Tecnai 20 transmission electron microscope (TEM). Element analysis was performed for carbon with a Perkin-Elmer 2400C elemental analyzer.

2.3. Galvanostatic Charge/Discharge Tests. Electrochemical Li-ion intercalation performances of the samples were evaluated in Li test cells. The cathode materials were prepared by mixing

10.1021/jp800040s CCC: $40.75
Published on Web 03/18/2008

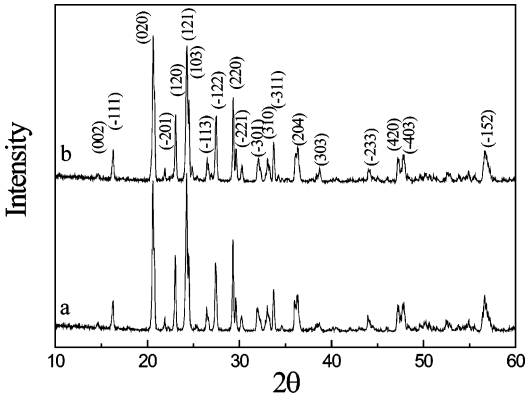

Figure 1. X-ray diffraction patterns of pure $Li_3V_2(PO_4)_3$ (a) and $Li_3V_2(PO_4)_3$@C composite (b).

the samples with acetylene black and polytetrafluoroethylene (PTFE) with a weight ratio of 85:10:5 in ethanol to ensure homogeneity. After the ethanol was evaporated, the mixture was rolled into a sheet, and the sheet was cut into circular strips of 8 mm in diameter. The strips were then dried at 100 °C for 10 h. Lithium metal was used as an anode. The electrolyte was composed of a 1 M $LiPF_6$ dissolved in ethylene carbonate (EC)/dimethyl carbonate (DMC)/ethylene methyl carbonate (EMC) with the volume ratio of 1:1:1. Test cells were assembled in an argon-filled dry glove box. The galvanostatic charge/discharge tests were performed with a Land CT2001 battery tester at different current densities in a voltage range of 3.0−4.5 V at 25 °C.

2.4. CV and EIS Measurements. Cyclic voltammograms (CVs) were conducted on a Zahner-Elektrik IM6e electrochemical workstation. The CV curves for the above test cells were recorded in a potential range of 3.0−4.5 V (vs Li^+/Li) at a scan rate of 0.05 mV s^{-1} at 25 °C. Electrochemical impedance spectroscopy (EIS) was also recorded on this electrochemical workstation with the frequency ranging from 10 kHz to 10 mHz and an AC signal of 5 mV in amplitude as the perturbation at 25 °C.

3. Results and Discussion

3.1. Sample Characterization. XRD patterns of pure $Li_3V_2(PO_4)_3$ and $Li_3V_2(PO_4)_3$@C composite are shown in Figure 1. The peaks can mainly be assigned to monoclinic $Li_3V_2(PO_4)_3$. Carbon is not detected in the pattern of $Li_3V_2(PO_4)_3$@C composite (Figure 1b); however, according to elemental analysis the carbon content in the composite is ~4.8%. Usually carbon obtained from glucose under hydrothermal condition is amorphous and cannot be detected through XRD even with higher amounts.

Figure 2 shows SEM images of pure $Li_3V_2(PO_4)_3$ and $Li_3V_2(PO_4)_3$@C composite. The pure $Li_3V_2(PO_4)_3$ sample has a spherical morphology that is ~400 nm in diameter, and the small particles show good crystallinity and homogeneity, compared with those synthesized via solid-state reactions or other sol−gel methods.[12,13] After carbon coating the particles are connected with each other within the carbon network.

TEM images of $Li_3V_2(PO_4)_3$@C composite are shown in Figure 3. The $Li_3V_2(PO_4)_3$ particle is encapsulated with amorphous carbon shell, similar to carbon-coated $LiMn_2O_4$ or silicon.[35,36] It can be seen that the thickness of the carbon shell is about 10 nm. The thickness of the carbon shell can be controlled by the hydrothermal reaction time and quantity of glucose. The high-resolution TEM image in Figure 3b clearly demonstrates the coexistence of two phases, i.e., $Li_3V_2(PO_4)_3$ and amorphous carbon.

3.2. Galvanostatic Charge/Discharge Measurements. The initial galvanostatic discharge/charge curves for Li/$Li_3V_2(PO_4)_3$@C and Li/$Li_3V_2(PO_4)_3$ test cells are shown in Figure 4, measured at a current density of 28 mAg^{-1} (C/5 rate) in the potential range of 3.0−4.5 V at 25 °C. Both cells exhibit three charge plateaus around 3.6, 3.7, and 4.1 V and correspondingly three discharge plateaus around 4.0, 3.7, and 3.6 V, which are identified as the two-phase transition processes during the electrochemical reactions. The initial discharge capacities for $Li_3V_2(PO_4)_3$ and $Li_3V_2(PO_4)_3$@C are 109.2 and 127.8 $mAhg^{-1}$, respectively. Even from the initial discharge capacity, the effect of the carbon shell is very apparent and even more significant from long-term cyclic charge/discharge performances at higher current density, as shown in Figure 5.

The discharge capacity of $Li_3V_2(PO_4)_3$@C is 125.9 $mAhg^{-1}$ after 50 cycles at a current density of 28 mAg^{-1}, much higher than pure $Li_3V_2(PO_4)_3$ (68.1 $mAhg^{-1}$ after 30 cycles), so the retention rate in discharge capacities is 98.5% for $Li_3V_2(PO_4)_3$@C after 50 cycles but only 62.8% for pure $Li_3V_2(PO_4)_3$ after 30 cycles. At a higher current density (140 mAg^{-1}, 1C rate), the retention rate still attains 96.2% for $Li_3V_2(PO_4)_3$@C. Therefore, the $Li_3V_2(PO_4)_3$@C composites have higher discharge capacity and better cyclic ability.

3.3. CV Measurements. The initial CV curves are shown in Figure 6 for the pure $Li_3V_2(PO_4)_3$ and $Li_3V_2(PO_4)_3$@C electrodes. There are three oxidation peaks and three reduction peaks in the potential range of 3.0−4.5 V for both electrodes, in agreement with the charge/discharge curves (Figure 4). The first two anodic peaks around 3.78 and 3.85 V correspond to removal of the first Li in two steps, since there is an ordered $Li_{2.5}V_2(PO_4)_3$ phase.[10] However, the second Li is extracted through one step around 4.26 V. The three cathodic peaks located around 3.68, 3.77, and 4.16 V are attributed to reinsertion of the two Li ions, associated with the V^{4+}/V^{3+} redox couple.

In Figure 6 there are some apparent differences between the two curves. First, the current density of the $Li_3V_2(PO_4)_3$@C electrode is higher than that of the pure $Li_3V_2(PO_4)_3$ electrode. For the coin-type cell systems the electrode can approximately be regarded as a flat one, and the peak current density is represented as follows: $i_p = 2.6 \times 10^5 n^{3/2} C_0 D^{1/2} \nu^{1/2}$, where n is the number of electrons transferred per molecule during the intercalation, C_0 is the concentration of lithium ions, D is the diffusion coefficient of lithium ions, and ν is the scan rate.[37,38] Since $i_p \propto D^{1/2}$, the diffusion coefficient of Li ions is higher in the $Li_3V_2(PO_4)_3$@C electrode than in the pure $Li_3V_2(PO_4)_3$ electrode. Second, as summarized in Table 1, the potential differences between anodic peaks and cathodic peaks are smaller in the $Li_3V_2(PO_4)_3$@C electrode, indicating enhancement of the reversibility in the electrode reaction due to the presence of a carbon shell in $Li_3V_2(PO_4)_3$@C electrodes.

3.4. EIS Measurement. The EIS measurements were performed for pure $Li_3V_2(PO_4)_3$ and $Li_3V_2(PO_4)_3$@C electrodes during different cycles when charged to 3.6 V, and the Nyquist plots are shown in Figure 7. In the first cycle (Figure 7a), both electrodes exhibit a semicircle in the high-frequency range and an inclined line in the low-frequency range. The high-frequency semicircle is assigned to the charge-transfer impedance in the electrode/electrolyte interface, and the inclined line corresponds to the lithium-ion diffusion process.[25,39,40] The charge-transfer impedances for pure $Li_3V_2(PO_4)_3$ and $Li_3V_2(PO_4)_3$@C electrodes are 940 and 230 Ω, respectively, which illustrates the charge-transfer impedances decreased greatly due to the presence of

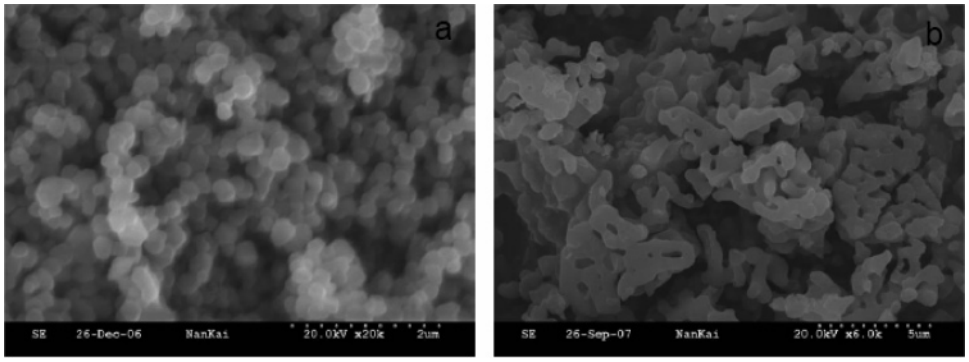

Figure 2. SEM images of pure $Li_3V_2(PO_4)_3$ (a) and $Li_3V_2(PO_4)_3$@C composite (b).

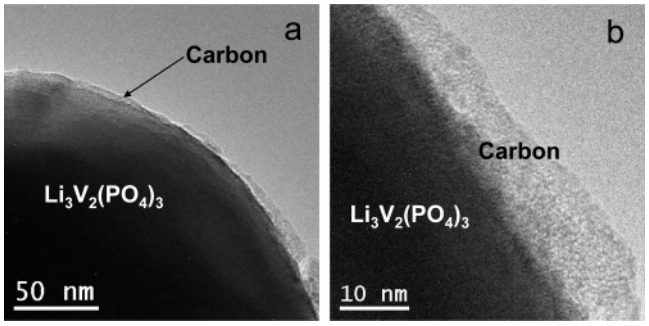

Figure 3. TEM image of $Li_3V_2(PO_4)_3$@C composite (a) and the corresponding high-resolution TEM image (b).

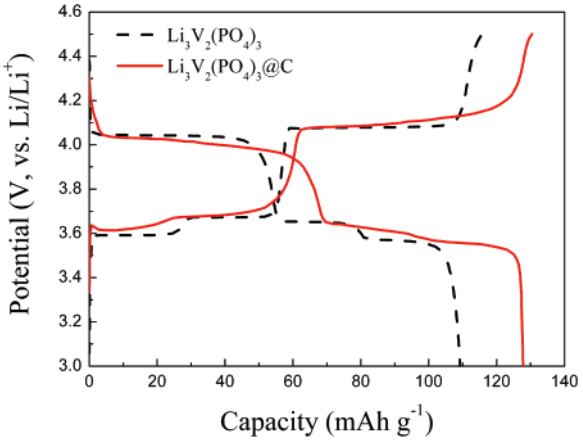

Figure 4. Typical charge/discharge curves of $Li_3V_2(PO_4)_3$ and $Li_3V_2(PO_4)_3$@C electrodes.

the carbon shell in $Li_3V_2(PO_4)_3$@C electrodes. During the 21st cycle (Figure 7b), the pure $Li_3V_2(PO_4)_3$ electrode has two semicircles; the high-frequency semicircle is attributed to the solid electrolyte interphase (SEI) film and contact resistance, and the semicircle in medium frequency is the charge-transfer impedance.[39] However, in this cycle the $Li_3V_2(PO_4)_3$@C electrode shows only one semicircle in the high-frequency range, since the presence of a carbon shell prevents formation of the SEI film in the surface of the $Li_3V_2(PO_4)_3$@C composites. The SEI film is a gel-like polymer containing LiF, Li_2CO_3, and lithium alkyl carbonate ($ROCO_2Li$) and leads to poor conductivity.[39,41] The EIS results demonstrate that the carbon shell can retard formation of the SEI film in the surface of the particles and also decrease the charge-transfer impedance; moreover, the carbon shell provides a good network for low-conductance $Li_3V_2(PO_4)_3$, so the electrochemical performances were improved greatly due to the core−shell structures in $Li_3V_2(PO_4)_3$@C composites.

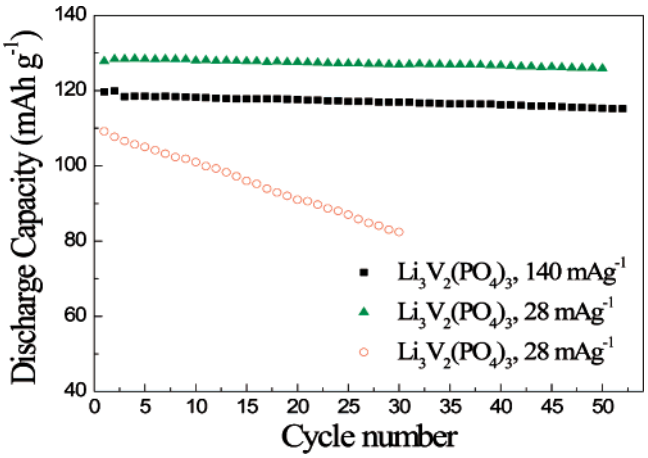

Figure 5. Cyclic performance of $Li_3V_2(PO_4)_3$ and $Li_3V_2(PO_4)_3$@C tested at different current densities at 25 °C.

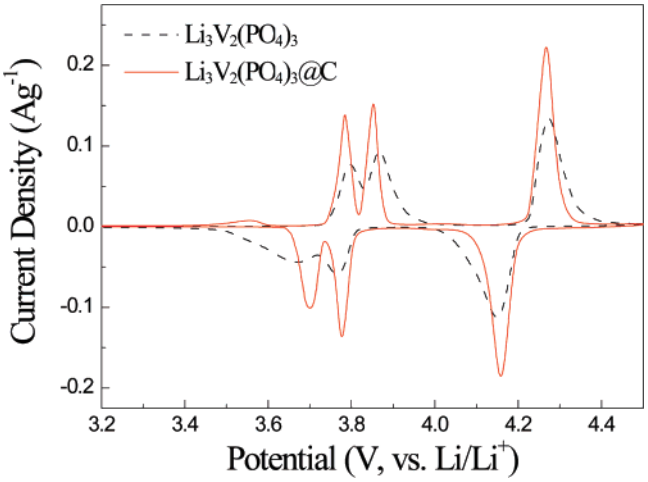

Figure 6. Cyclic voltammograms of $Li_3V_2(PO_4)_3$ and $Li_3V_2(PO_4)_3$@C electrodes at the first cycle.

The $Li_3V_2(PO_4)_3$@C composites have better electrochemical performance, which can be attributed to the carbon shell. As we know, polyanion Li^+ intercalation materials have lower electrical conductivity; however, as for the $Li_3V_2(PO_4)_3$@C composites, the carbon shell provides a network for $Li_3V_2(PO_4)_3$ particles and accordingly increases the electrical conductivity as well as lithium-ion diffusion. Also, formation of the SEI film was retarded due to the existence of the carbon shell according to the EIS analysis. As proposed initially, core−shell materials used in Li-ion batteries were expected to combine the functions of both core and shell parts and improve the general performances of the composites. For example, core−shell cathode materials with $Li[Ni_{0.8}Co_{0.1}Mn_{0.1}]O_2$ as cores and $Li[Ni_{0.5}Mn_{0.5}]$-

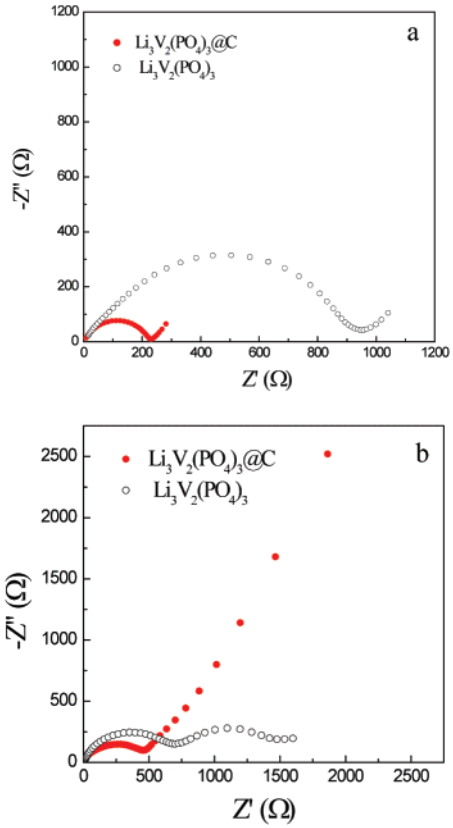

Figure 7. Nyquist plots of $Li_3V_2(PO_4)_3$ and $Li_3V_2(PO_4)_3$@C electrodes measured at the charge potential of 3.6 V during the first cycle (a) or 21st cycle (b).

TABLE 1: Potential Differences between the Anodic and Cathodic Peaks for $Li_3V_2(PO_4)_3$ and $Li_3V_2(PO_4)_3$@C Electrodes

	ΔE_{O1-R1} (V)	ΔE_{O2-R2} (V)	ΔE_{O3-R3} (V)
$Li_3V_2(PO_4)_3$@C	0.086	0.086	0.111
$Li_3V_2(PO_4)_3$	0.124	0.104	0.127

O_2 as shells were reported to deliver high capacity from the $Li[Ni_{0.8}Co_{0.1}Mn_{0.1}]O_2$ core and a high thermal stability due to the $Li[Ni_{0.5}Mn_{0.5}]O_2$ shell.[22] Core−shell anode materials such as Si or transition-metal oxides as cores and carbon as shell can alleviate the volume change during lithium intercalation and deintercalation.[23−25] Core−shell structures proposed in this work may promote the practical applications of $Li_3V_2(PO_4)_3$ cathode materials to Li-ion batteries.

4. Conclusion

Core−shell $Li_3V_2(PO_4)_3$@C composites were synthesized via a sol−gel route and a subsequent hydrothermal procedure. TEM images validated the $Li_3V_2(PO_4)_3$ particles encapsulated with an amorphous carbon shell of ~10 nm in thickness. The $Li_3V_2(PO_4)_3$@C composites exhibited enhanced discharge capacity and cyclic ability. The discharge capacity of $Li_3V_2(PO_4)_3$@C is 127.8 mAh g^{-1} in the first cycle and 125.9 mAh g^{-1} in the 50th cycle at a current density of 28 mA g^{-1}, and the retention rate of discharge capacities is 98.5%, much higher than those of pure $Li_3V_2(PO_4)_3$. Even at higher current density (140 mA g^{-1}), the retention rate still reaches 96.2% for $Li_3V_2(PO_4)_3$@C composites. Electrochemical measurements disclosed that the carbon shell retarded formation of the SEI film in the surface of the particles and improved the electrical conductivity and lithium-ion diffusion. Core−shell nanostructured materials are very effective for promoting transition-metal phosphates as cathode materials in Li-ion batteries.

Acknowledgment. This work was supported by the 973 National Basic Research Program (2002CB211800), the 863 National High Technology Research and Development Program (2007AA03Z225), and Tianjin Natural Science Foundation (06YFJMJC13300) in China.

References and Notes

(1) Padhi, A. K.; Najundaswamy, K. S.; Goodenough, J. B. *J. Electrochem. Soc.* **1997**, *144*, 1118.
(2) West, W. C.; Whitacre, J. F.; Ratnakumar, B. V. *J. Electrochem. Soc.* **2003**, *150*, A1660.
(3) Delacourt, C.; Poizot, P.; Morcrette, M.; Tarascon, J. M.; Masquelier, C. *Chem. Mater.* **2004**, *16*, 93.
(4) Chung, S.-Y.; Bloking, J. T.; Chiang, Y. M. *Nat. Mater.* **2002**, *1*, 123.
(5) Amine, K.; Yasuda, K.; Yamachi, M. *Electrochem. Solid-State Lett.* **2000**, *3*, 178.
(6) Xie, H. M.; Wang, R. S.; Ying, J. R.; Zhang, L. Y.; Jalbout, A. F.; Yu, H. Y.; Yang, G. L.; Pan, X. M.; Su, Z. M. *Adv. Mater.* **2006**, *18*, 2609.
(7) Yamada, A.; Chung, S. C. *J. Electrochem. Soc.* **2001**, *148*, A960.
(8) Hu, Y. Q.; Doeff, M. M.; Kostecki, R.; Finonesa, R. *J. Electrochem. Soc.* **2005**, *151*, A1279.
(9) Shin, H. C.; Chob, W. I.; Jang, H. *J. Power Sources* **2006**, *159*, 1383.
(10) Saidi, M. Y.; Barker, J.; Huang, H.; Sowyer, J. L.; Adamson, G. *J. Power Sources* **2003**, *119−112*, 266.
(11) Hung, H.; Yin, S. C.; Kerr, T.; Taylor, N.; Nazar, L. F. *Adv. Mater.* **2002**, *14*, 1525.
(12) Ren, M. M.; Zhou, Z.; Li, Y. Z.; Gao, X. P.; Yan, J. *J. Power Sources* **2006**, *162*, 1357.
(13) Li, Y. Z.; Zhou, Z.; Ren, M. M.; Gao, X. P.; Yan, J. *Electrochim. Acta* **2006**, *51*, 6498.
(14) Yin, S. C.; Grond, H.; Strobel, P.; Huang, H.; Nazar, L. F. *J. Am. Chem. Soc.* **2000**, *125*, 326.
(15) Li, Y. Z.; Zhou, Z.; Gao, X. P.; Yan, J. *Electrochim. Acta* **2007**, *52*, 4922.
(16) Yin, S. C.; Grondey, H.; Strobel, P.; Anne, M.; Nazar, L. F. *J. Am. Chem. Soc.* **2003**, *125*, 10402.
(17) Fu, P.; Zhao, Y. M.; An, X. N.; Dong, Y. Z.; Hou, X. M. *Electrochim. Acta* **2007**, *52*, 5281.
(18) Chen, Q. Q.; Wang, J. M.; Tang, Z.; He, W. C.; Shao, H. B.; Zhang, J. Q. *Electrochim. Acta* **2007**, *52*, 5251.
(19) Barker, J.; Saidi, M. Y.; Swoyer, J. L. *J. Electrochem. Soc.* **2003**, *150*, A1394.
(20) Li, Y. Z.; Zhou, Z.; Gao, X. P.; Yan, J. *J. Power Sources* **2006**, *160*, 633.
(21) Barker, J.; Gover, P. K. B.; Burns, P.; Bryan, A. *Electrochem. Solid-State Lett.* **2005**, *8*, A285.
(22) Sun, Y. K.; Myung, S. T.; Kim, M. H.; Prakash, J.; Amine, K. *J. Am. Chem. Soc.* **2005**, *127*, 13411.
(23) Lee, K. T.; Jung, Y. S.; Oh, S. M. *J. Am. Chem. Soc.* **2003**, *125*, 5652.
(24) Fu, L. J.; Liu, H.; Zhang, H. P.; Li, C.; Zhang, T.; Wu, Y. P.; Holze, R.; Wu, H. Q. *Electrochem. Commun.* **2006**, *8*, 1.
(25) Huang, X. H.; Tu, J. P.; Zhang, C. Q.; Chen, X. T.; Yuan, Y. F.; Wu, H. M. *Electrochim. Acta* **2007**, *52*, 4177.
(26) Li, M.; Lu, Q. H.; Nuli, Y.; Qian, X. F. *Electrochem. Solid-State Lett.* **2007**, *10*, K33.
(27) Park, B.-C.; Bang, H. J.; Amine, K.; Jung, E.; Sun, Y.-K. *J. Power Sources* **2007**, *174*, 658.
(28) Sun, X. M.; Liu, J. F.; Li, Y. D. *Chem. Mater.* **2006**, *18*, 3486.
(29) Wang, K.; He, X. M.; Wang, L.; Ren, J. G.; Jiang, C. Y.; Wan, C. R. *Solid State Ionics* **2007**, *178*, 115.
(30) Jung, Y. S.; Lee, K. T.; Oh, S. M. *Electrochim. Acta* **2007**, *52*, 7061.
(31) Kwon, Y.; Kim, H.; Doo, S.-G.; Cho, J. *Chem. Mater.* **2007**, *19*, 982.
(32) Lee, H.; Cho, J. *Nano Lett.* **2007**, *7*, 2638.
(33) Sun, Y. K.; Myung, S. T.; Park, B. C.; Amine, K. *Chem. Mater.* **2006**, *18*, 5159.
(34) Sun, X. M.; Li, Y. D. *Angew. Chem., Int. Ed.* **2004**, *43*, 597.
(35) Han, A. R.; Kim, T. W.; Park, D. H.; Hwang, S.-J.; Choy, J.-H. *J. Phys. Chem. C* **2007**, *111*, 11347.

(36) Ng, S. H.; Wang, J.; Wexler, D.; Chew, S. Y.; Liu, H. K. *J. Phys. Chem. C* **2007**, *111*, 11131.
(37) Liu, H.; Fu, L. J.; Zhang, H. P.; Gao, J.; Li, C.; Wu, Y. P.; Wu, H. Q. *Electrochem. Solid-State Lett.* **2006**, *9*, A529.
(38) Bard, A. J.; Faulkner, L. R. *Electrochemical Methods*; Wiley: New York, 1980; p 213.
(39) Takahashi, M.; Tobishima, S.-I.; Takei, K.; Sakurai, Y. *Solid State Ionics* **2002**, *148*, 283.
(40) Yang, S. B.; Song, H. H.; Chen, X. H. *Electrochem. Commun.* **2006**, *8*, 137.
(41) Grugeon, S.; Laruelle, S.; Herrera-Urbina, R.; Dupont, L.; Poziot, P.; Tarascon, J. M. *J. Electrochem. Soc.* **2001**, *148*, A285.